Atmospheric
Chemistry
and Physics

Open Access

EGU

Supplement of

An organic crystalline state in ageing atmospheric aerosol proxies: spatially resolved structural changes in levitated fatty acid particles

Adam Milsom et al.

Correspondence to: Christian Pfrang (c.pfrang@bham.ac.uk)

S1. Acid-Soap Characterisation

	Lamellar *d*-spacing / nm (uncertainty)	
	This work [21 °C]	Literature [*T*]***
OA:SO (1:1) Acid–Soap	4.5773 (0.0001)*	4.61 (0.05) [5 °C](Tandon et al., 2001)
Sodium Oleate	4.35 (0.02)**	4.51 (0.05) [15 °C](Tandon et al., 2000b)
Oleic Acid	Liquid at this temperature	4.14 (0.05) [5 °C](Tandon et al., 2000a)

Table S1. Comparison of measured lamellar *d*-spacings for the oleic acid–sodium oleate acid–soap complex with pure sodium oleate and oleic acid (*:levitated particle; **: capillary coating, ***: bulk sample; OA: oleic acid; SO: sodium oleate).

	WAXS Spacings / nm (uncertainty)							
This work (21 °C)	0.467 (0.001)	0.455 (0.004)	0.444 (0.006)	0.407 (0.001)	0.399 (0.001)	0.378 (0.002)	0.369 (0.001)	0.363 (0.001)
Tandon et al. (Tandon et al., 2001) **(5 °C)**	0.470	0.462	0.452	0.404	0.396	0.376	0.368	0.362
Tandon et al.(Tandon et al., 2001) **(30 °C)**	0.471	0.451	0.412	0.408	0.400	0.379	0.371	0.365

Table S2. WAXS spacings measuring the repeat distance between scattering planes in the hydrophobic tail.

Table S1 compares our measured *d*-spacing with that obtained by Tandon *et al.* for the same system, but in a bulk sample and at a lower temperature. This table also includes the spacings of oleic acid and sodium oleate at low temperatures (Tandon et al., 2000a, 2000b). The value for the acid–soap complex is significantly different from the oleic acid and sodium oleate *d*-spacings. It is however within the error of the 4.61 ± 0.05 nm quoted by Tandon *et al.*(Tandon et al., 2001) for a bulk sample. The substantial difference in uncertainty is due to the difference in techniques used: the present study utilised synchrotron radiation many times more intense than the X-rays from the laboratory-based powder diffraction instrument used in the literature. The number quoted in this study therefore has much better statistics associated with it.

The WAXS spacings measured in this study in general agree with the literature values (Table S2). Signals in the WAXS region suggest that a sample is crystalline, exhibiting shorter distance order in addition to the longer distance lamellar spacings. These characteristic spacings measure the sub-cell packing arrangements. Tandon *et al.* computed three sets of sub-cell parameters which accommodate the spectroscopically-deduced parallel fatty acid chain packing, all with $O_{\parallel}$ sub-cell symmetry (Tandon et al., 2001).

The melting temperature for this acid–soap complex has been reported as ~ 32 °C (Tandon et al., 2001). Exploiting the birefringent property of the acid–soap complex, a POM experiment was carried out on the acid–soap sample used in this study along with oleic acid–sodium oleate mixtures of varying ratios. The decomposition of the acid–soap structure occurred in agreement with the literature at ~ 32 °C. Further details are provided in the Supplement sect. S2.

Oleic acid and sodium oleate have markedly different Raman spectra (Fig. S1). The packing of the alkyl chains in sodium oleate is more ordered than that of oleic acid. This is exhibited by the difference in peak profile in the C–H stretching region (~ 2840–3050 cm^{-1}) (Tandon et al., 2000a, 2000b, 2001). The acid–soap complex has features similar to sodium oleate due to its crystallinity. However, the acid–soap complex spectrum is clearly distinct from those of its constituent species (see Fig. S1: panel (a) *vs.* (b)–(d)).
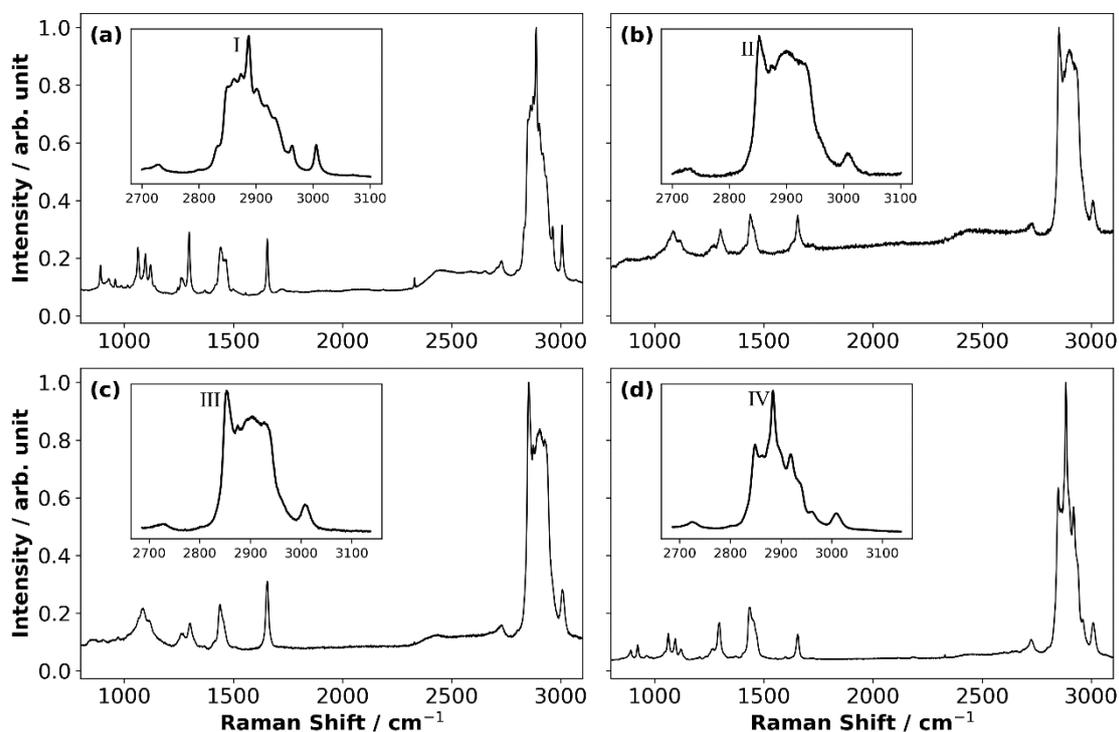
Figure S1. Raman spectra of (a) the acid–soap complex; (b) a bulk mixture of oleic acid:sodium oleate (1:1 wt) 30 wt % in water - the hexagonal LLC phase; (c) oleic acid and (d) sodium oleate. All samples deposited on microscope slides. C–H stretching region is enlarged and displayed as an inset. Key peaks associated with alkyl chain ordering are labelled: I = 2887 cm^{-1}, II & III = 2854 cm^{-1} and IV = 2884 cm^{-1}.

Figure S1 shows a comparison of the acid–soap complex (panel (a)) and its components (panels (c) and (d)). The Raman spectrum for a bulk LLC hexagonal phase (confirmed by SAXS) of oleic acid:sodium oleate (1:1 wt) 30 wt % in H$_2$O is also presented for comparison (panel (b)). The strong peak at 2887 cm^{-1} is characteristic of the ordered packing of the acid–soap complex alkyl chains and is similar to the findings of Tandon *et al* (Tandon et al., 2001), distinguishing it from its components. The oleic acid and liquid crystal spectra exhibit a stronger peak at 2854 cm^{-1} with the peak originally at 2887 cm^{-1} significantly weaker, up-shifted and broadened, arising from the disordered state of the alkyl chains in both of these systems. Additionally, there are sharp C–C stretching peaks between ~ 1050–1150 cm^{-1} which suggest

that there are multiple trans conformers in the hydrocarbon chain (Tandon et al., 2001). Raman spectra of levitated acid–soap complex particles exhibited peaks in similar positions, however these spectra were subject to very high background scattering (see Supplement sect. S4). Superimposed Raman spectra of the C–H stretching region of these components are presented in the Supplement (Fig. S2).
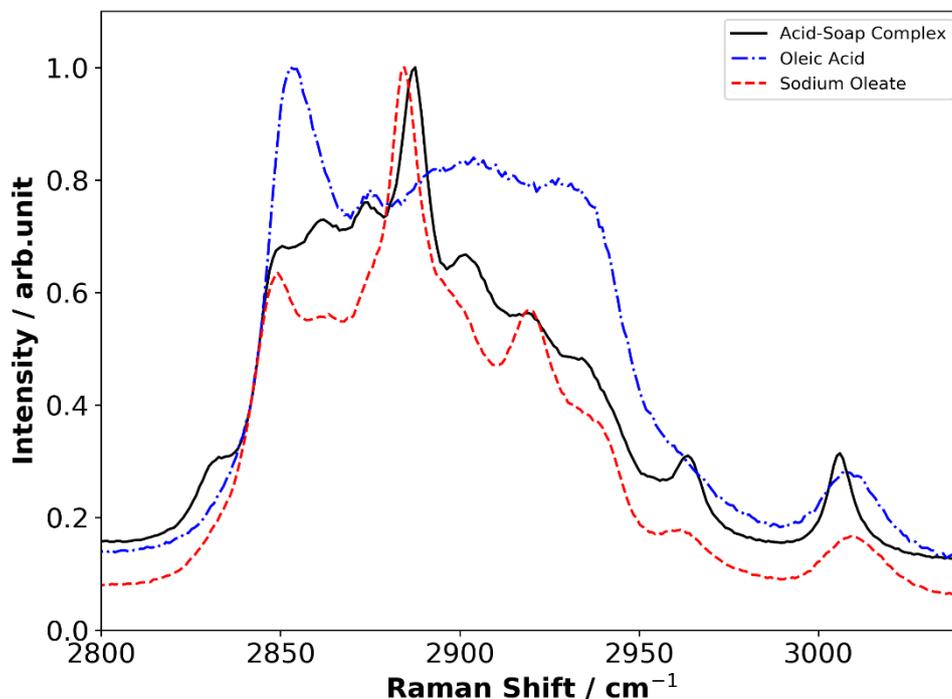
Figure S2. Superimposed Raman spectra of the 2800-3100 cm^{-1} region exhibiting differences in peak positions.

The carboxylate C=O bond peak is strong in IR spectroscopy. The position and intensity of this peak eludes to the environment the C=O bond is found in. This is structure-dependent: both oleic acid and sodium oleate have carboxyl peaks; oleic acid has its peak at 1707 cm^{-1}, while sodium oleate has its peak shifted by nearly 150 cm^{-1} to 1558 cm^{-1} (see Fig. S3).
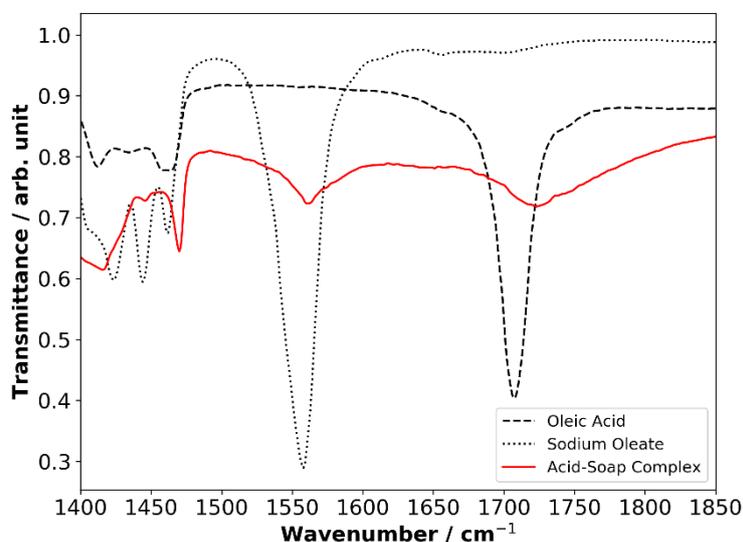
Figure S3. IR spectra of the acid–soap complex, oleic acid and sodium oleate. The CH_2 scissoring region is in the range of 1400-1500 cm^{-1}. The C=O bond peak region is in the range of 1500-1800 cm^{-1}.

The acid–soap complex exhibits a mixture of these two C=O/(–CO_2)⁻-related peaks. The carboxyl signal has been shifted slightly higher to 1712 cm^{-1} and is broader, consistent with the findings of Tandon *et al.*(Tandon et al., 2001). The broadening and partial disappearance of the two signals associated with oleic acid and sodium oleate suggest that the carboxylate groups are involved in hydrogen bonding, reported previously for similar complexes: sodium palmitate–palmitic acid(1:2)(Lynch et al., 1996) and $C_4 - C_{24}$ (1:1) acid–soap complexes (Mantsch et al., 1994).

The appearance of an un-split signal in the CH_2 scissoring region at 1469 cm^{-1} suggests the parallel chain arrangement as opposed to a perpendicular arrangement found in other acid–soaps (Lynch et al., 1996; Tandon et al., 2001). This region of the acid–soap IR spectrum is significantly different to its components.

S2. SAXS/WAXS of the Levitated Particle Centre during Humidity Changes
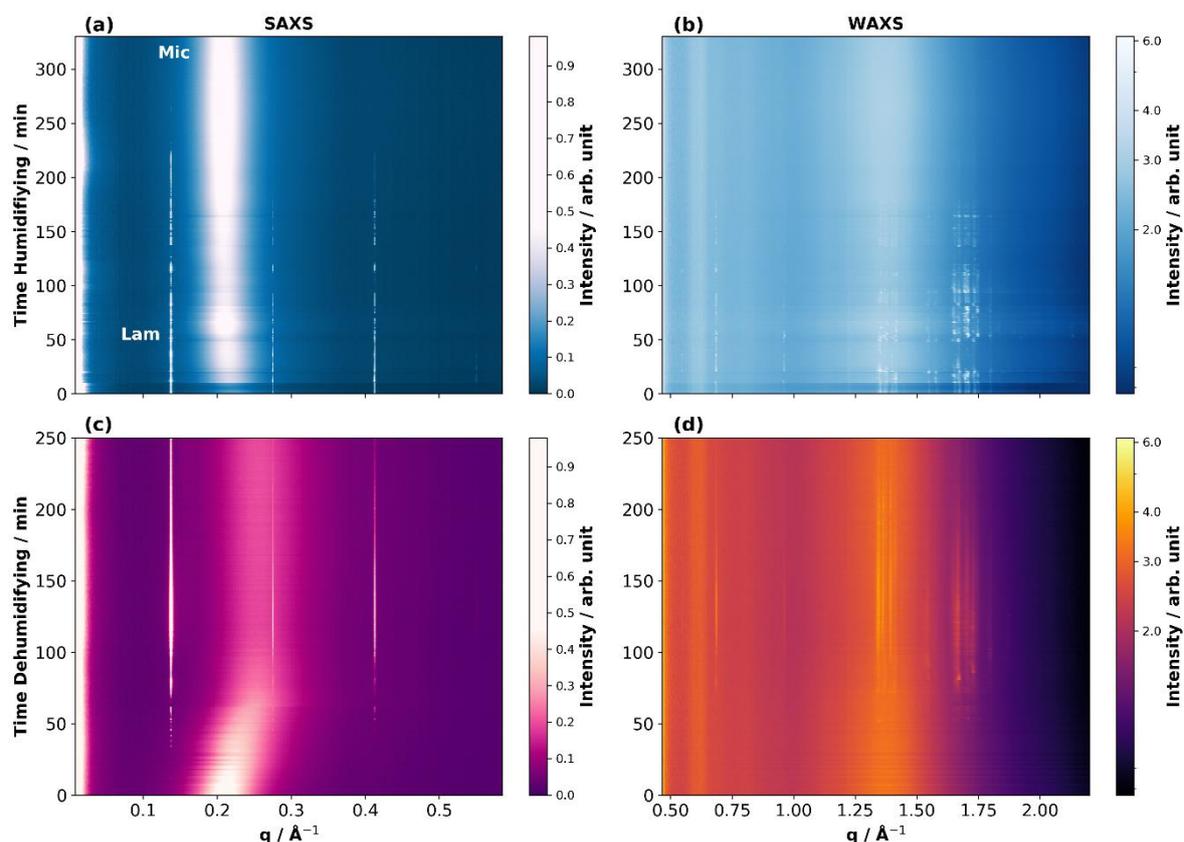
Figure S4. Evolution of the 1–D SAXS and WAXS patterns at the centre of a levitated acid–soap complex particle during humidification to 90 % RH (a) & (b) and dehumidification from 90 % RH to ~ 38 % RH (c) & (d). Peak positions for both SAXS and WAXS patterns are analogous to those in Fig. 1 – main text. The sharp first lamellar peak is labelled as 'Lam' and the broad inverse micellar peak is labelled as 'Mic' in panel (a) for clarity.

S3. Polarising Optical Microscopy (POM) – Thermal Decomposition of the Acid–Soap Complex

The oleic acid-sodium oleate acid–soap complex is reported to have a thermal decomposition temperature of ~ 32 °C (Tandon et al., 2001). As this complex is birefringent, it is possible to view it using cross-polarised light. The crystals exhibit a bright pattern (Fig. S5). Using a heating stage, it was possible to heat the sample from room temperature to the decomposition temperature reported in the literature.
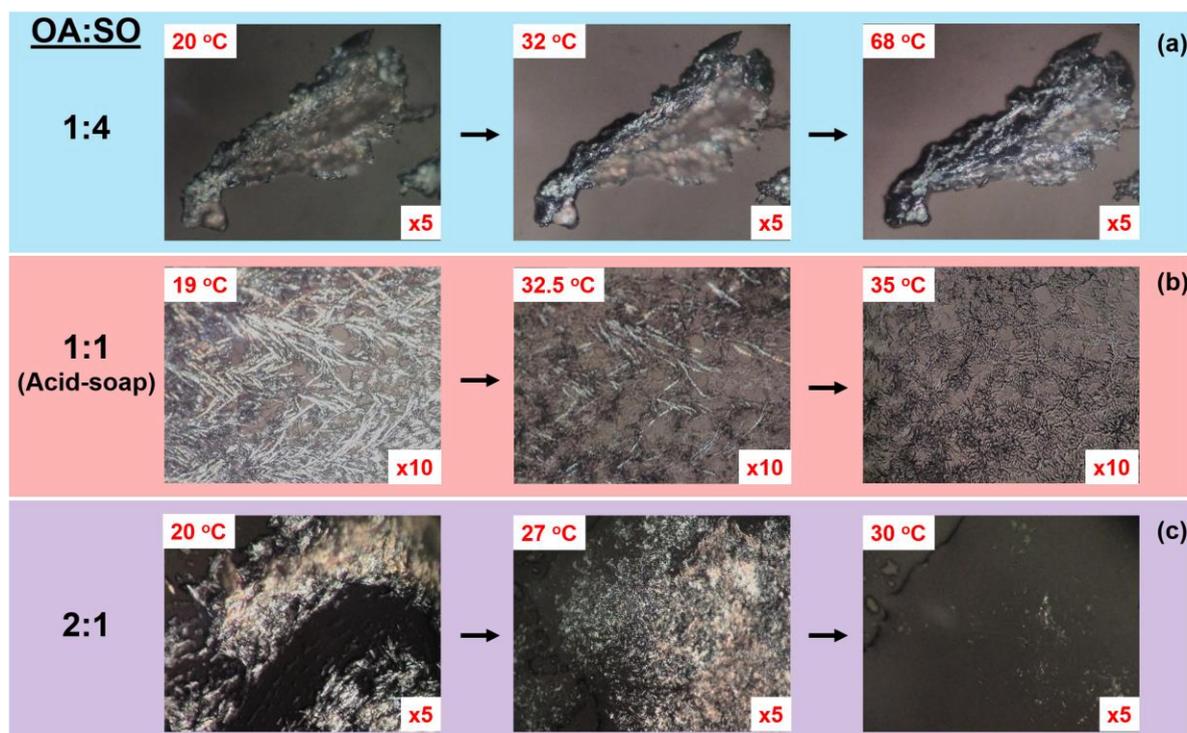
Figure S5. Polarising microscopy-temperature experiments of differing oleic acid:sodium oleate weight ratios deposited from ethanol onto microscope slides. OA = Oleic acid, SO = Sodium oleate. (a) 1: 4, (b) 1:1 (acid-soap complex) and (c) 2:1. RH ~ 50 %.

The acid–soap complex clearly starts to break down at ~ 32 °C. The pattern started to disappear rapidly once the temperature approached this value. No more birefringence was observed and the sample became 'dark'. This is a qualitative visual confirmation of the literature's observations obtained by Raman microscopy and X-ray diffraction. On inspection of the reported literature phase diagram, the acid-soap at this composition breaks down and forms an isotropic liquid (Tandon et al., 2001).

Two other oleic acid:sodium oleate ratios were made and tested in the same way, 2:1 and 1:4. Interestingly, the 2:1 ratio mixture became fluid at ~ 27 °C and lost its birefringence at ~ 30 °C. This is consistent with the phase diagram for the dry oleic acid/sodium oleate system. According to the reported phase diagram, this system becomes an isotropic liquid above the decomposition temperature and the decomposition temperature decreases as a function of the amount of oleic acid in the system (Tandon et al., 2001). The 1:4 system was heated to 68 °C. Some of the birefringence disappeared at ~ 32 °C. This is ascribed to the acid–soap complex in this system breaking down. The sample remained birefringent for the whole

experiment, suggesting that only sodium oleate was left in the crystalline state as its melting point is > 200 °C.

S4. Raman Spectra of the Levitated Acid-Soap Complex
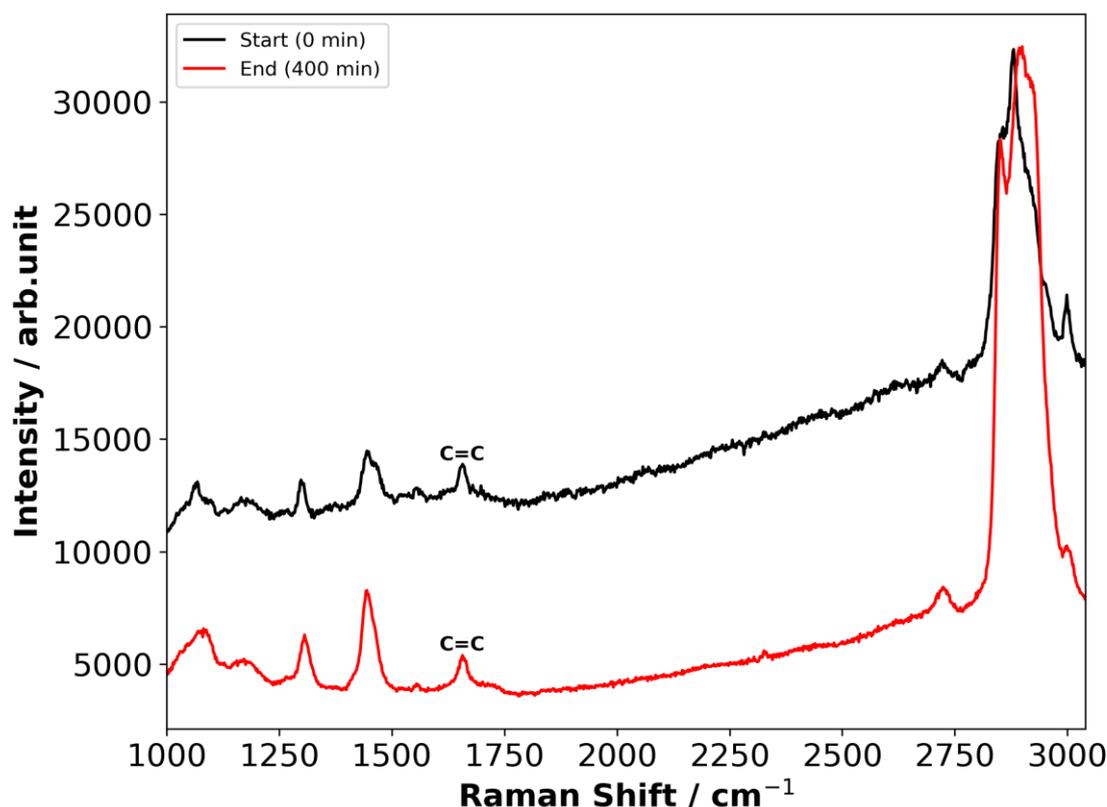
Figure S6. Raman spectra of the levitated acid-soap complex before and after ozonolysis for 400 min ($[O_3]$ = 51.9 ± 0.5 ppm). The carbon-carbon double bond peak used to measure reaction kinetics is labelled.

Figure S6 presents the Raman spectrum before and after ozonolysis. Note that the plot is not adjusted in order to stack the spectra, meaning that there is a significantly high background signal at the beginning of the experiment compared with the end. This is thought to be due to the high background scattering encountered when measuring Raman spectra of solid crystalline material such as the acid-soap complex.

The C=C bond has decreased in intensity compared to the C-H peak observed at ~ 1442 cm^{-1} indicating that oleic acid has reacted. However, there is still a clear signal remaining at the end of the experiment corresponding to 34.0 ± 8.5 % of oleic acid remaining in the particle (see main text Fig. 3). Note the change in profile of the region 2750-3050 cm^{-1}. This is evidence of the acid-soap complex breaking down and is presented and discussed in the *Evolution of the SAXS pattern during Ozonolysis* section of the main text.

S5. Optical Images of a Levitated Sodium Oleate Particle - Humidification
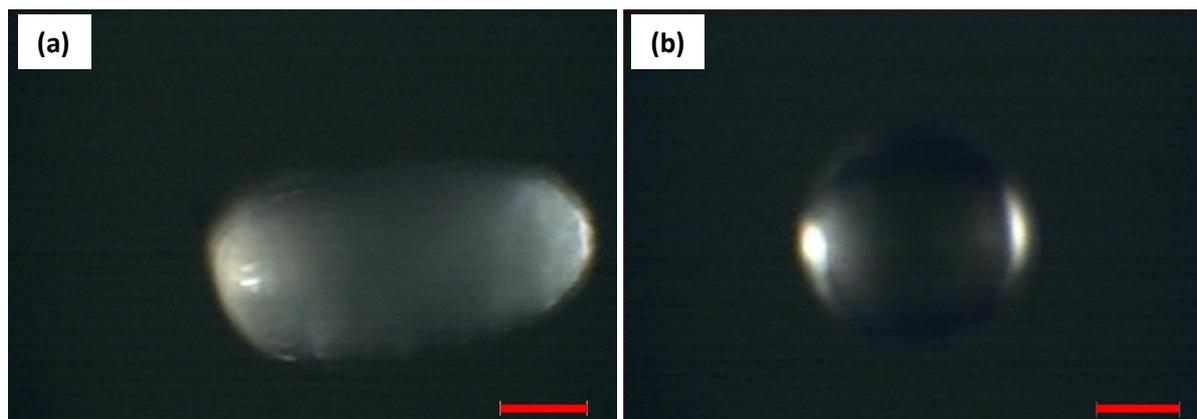
Figure S7. Two optical images of a levitated sodium oleate particle before humidification (a) and after humidification to > 90 % RH for ~ 3 h (b). Red scale bar represents 50 µm.

A particle of sodium oleate was levitated at ~ 50 % RH and exposed to > 90 % RH for a prolonged period (~ 3 h) in order to demonstrate the change in size and shape of a solid hygroscopic particle, such as sodium oleate, after water uptake. The deliquescence point of sodium oleate has been measured to be 88 ± 2 % (Nájera, 2007). There is a clear difference in size and shape between a dry and deliquesced particle.

S6. Low-q SAXS Evidence for High-Molecular-Weight Product Formation during Ozonolysis
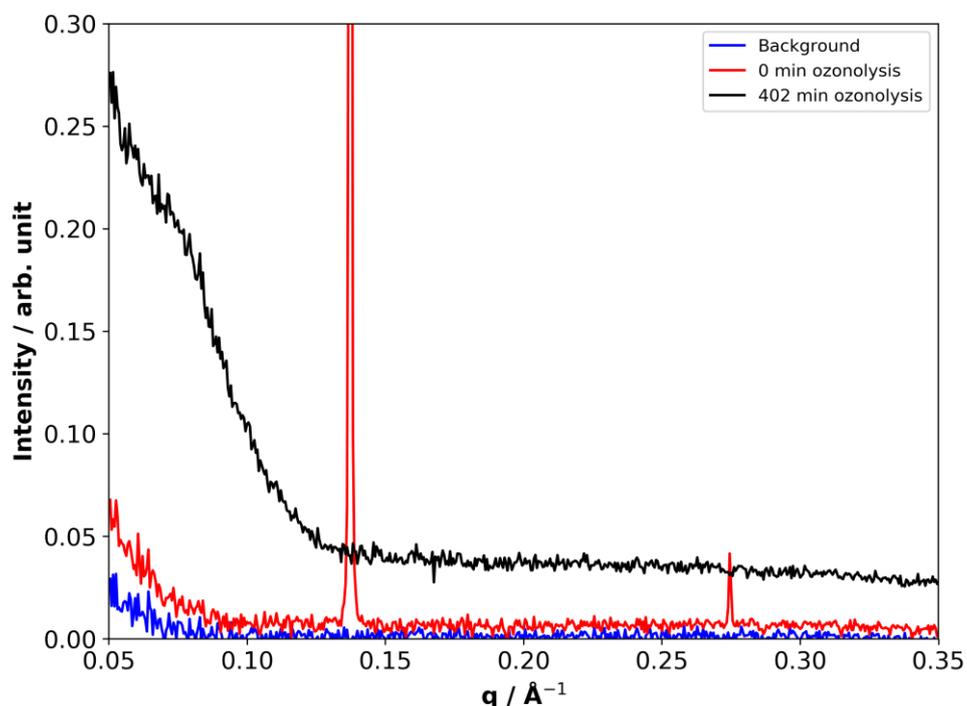
Figure S8. SAXS patterns of a levitated acid-soap complex before and after ozonolysis compared with an empty-levitator background. There is a clear increase in low-q scattering as a result of ozonolysis. [O_3] = 52 ± 0.5 ppm.

Figure S8 clearly shows an increase in low-q SAXS signal and the appearance of a shoulder at ~ 0.07 Å^{-1} as a result of ozonolysis. Low-q scattering signals are observed for species with large repeat distances between equivalent scattering centres. Structures formed by polymeric molecules exhibit patterns at low q due to the larger size of those molecules compared to our fatty acid precursors (Meznarich et al., 2011). As the particle is a complex mixture of products, it is not possible to discern much about the structure from this scattering curve because of the impure nature of the scattering phase. Better low-q resolution would be required to study structures with larger repeat distances than the self-assembled structures of smaller molecules (oleic acid-sodium oleate) we focus on in this study. This can be achieved by increasing the sample-to-detector distance of the SAXS setup – not practicable during a time-critical synchrotron beamtime experiment. Nevertheless, the presence of a structure with low-q scattering peak even after ozonolysis suggests that products themselves exhibit some ordering.

S7. POM of the Humidified and Dehumidified Acid–Soap Complex

Visual and spectroscopic evidence for a phase separation was obtained using POM (see section S3) and Raman microscopy; a summary of which is in Fig. S9. A film of the acid–soap complex was deposited on a microscope slide and initially allowed to dry over 6 days. A POM picture was taken at room RH (~ 50 %, Fig S9(a)). The acid–soap complex sample was birefringent with characteristic lamellar "streaks". The sample was then exposed to a saturated humidity chamber which was created by half-filling a small container with ultrapure water and suspending the microscope slide within it. The sample was left in the chamber for 7 days.
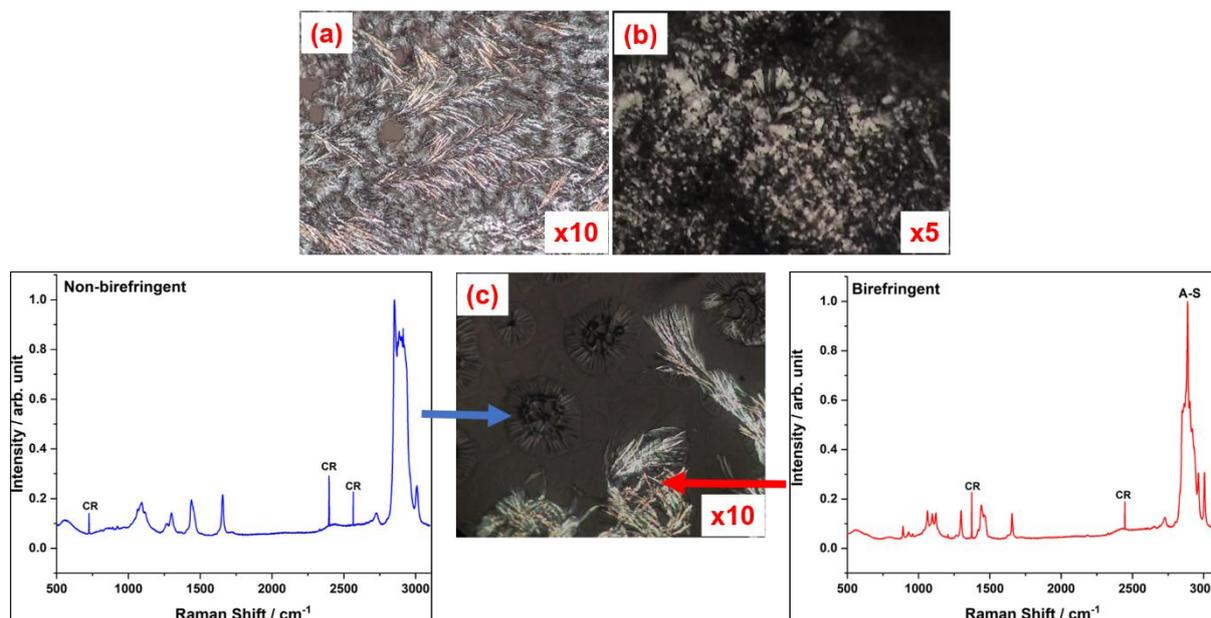
Figure S9. POM images of the oleic acid:sodium oleate (1:1 wt) acid–soap complex. (a) At ~ 50 % RH, showing a birefringent needle-like/streaky lamellar pattern. (b) Immediately after removal from the saturated humidity chamber. A "charcoal-like" pattern is observed, suggesting a hexagonal phase. (c) 5 h after removal from humidity chamber. Birefringent needles have returned along with a non-birefringent phase. Raman spectra of each portion presented both sides – A–S = Acid–Soap Complex Peak, CR = Cosmic Ray.

A POM picture was taken immediately after removal from the humidity chamber and exhibited a "charcoal" texture under the polarising microscope known to be the hexagonal phase texture for this system (Mele et al., 2018) (Fig. S9(b)), which disappeared within ~ 5 min of being in room RH (~ 50 %). This is evidence for an inverse hexagonal lyotropic liquid crystal phase which has been shown to form in the *potassium* oleate variant of this acid–soap complex (Cistola et al., 1986) and also for the oleic acid/sodium oleate/water/NaCl solution system (Engblom et al., 1995; Mele et al., 2018; Pfrang et al., 2017; Seddon et al., 1990). The fast disappearance of this texture suggests that this phase exists at high water content. Indeed, the hexagonal phase has been observed in our offline SAXS experiments using bulk mixtures of this fatty acid composition in excess water (Fig. S12). The hexagonal phase was not observed in the SAXS patterns for levitated acid–soap complex particles. The POM samples were allowed to equilibrate for a week at > 90 % RH as opposed to 340 min for the levitated particles. Longer experiments are not practicable during a synchrotron beamtime. Therefore the inverse hexagonal phase may indeed form in a levitated acid-soap complex particle if left to equilibrate over a period of days.

5 h after removal from the humidification chamber into room RH (~ 50 %), a phase separation is observed. Polarising microscopy pictures, in combination with Raman spectra of the birefringent and non-birefringent regions, confirm that there are two physically-distinct phases present after a 5 h equilibration time. It is suggested that the birefringent phase, now presented as needle-like structures, is the acid–soap complex. This is confirmed by the Raman spectrum taken of this region (Fig. S9(c)). The non-birefringent region is assumed to be the inverse micellar phase, possibly with an excess of oleic acid as there was an excess to begin with.

We believe that the glass substrate did not affect the structure formed on the glass slides. The Raman spectrum of the acid-soap complex exhibits the same strong peak at ~ 2887 cm-1 as demonstrated in the characterisation section (sect. S1) and in levitated particles of the same mixture (Fig. S4). The formation of the inverse hexagonal phase at high humidity is consistent with a bulk mixture of this organic composition with excess water (see sect. S9), where the sample vial would not have affected the resulting nanostructure. The non-birefringent phase observed after the humidification-dehumidification experiment is likely the inverse micellar phase, observed in levitated particles after humidity changes (see Fig. 1(l) in the main text and Fig. S4(c)). As we are confident that the glass substrate does not affect the observed structures, one can reasonably assume that this is the case for this non-birefringent phase.

S8 Water content determination and water uptake/loss model
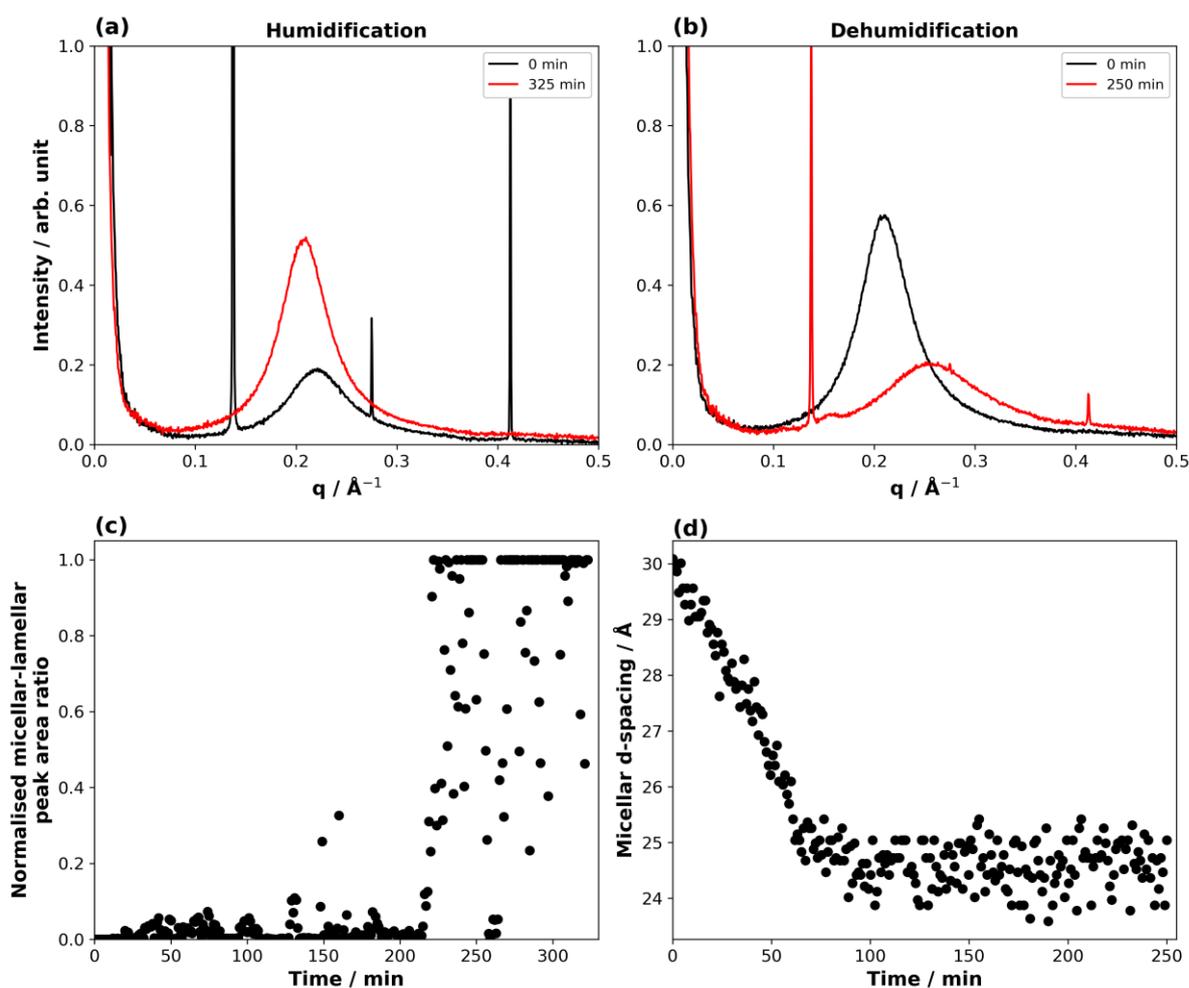
Figure S10. (a) & (b) SAXS patterns during humidification and dehumidification at the centre of the particle. Initial and final patterns presented to show the broad micellar peak centre (~ 0.20-0.26 Å^{-1}) change position and intensity relative to the lamellar peak. (c) normalised micellar-lamellar peak ratio vs time humidifying; (d) inverse micellar *d*-spacing vs time humidifying and dehumidifying.

As described in the *Water Diffusion Gradient during Humidity Change* section of the main text, the micellar-lamellar peak area ratio and micellar *d*-spacing were chosen as measures of water content for humidification and dehumidification, respectively. Micellar-lamellar peak area ratio data were noisy, especially once the particle had taken up a relatively large amount of water at ~ 230 min (Fig. S10(c)). Experimental micellar-lamellar peak area ratios which were greater than the median of ratios from 230 min onwards (*i.e.* the average maximum micellar-lamellar peak area ratio, accounting for the occasional large fluctuation) were set as that median value (2315) and this was assumed to be the value at maximum water content – all values are normalised to this number in Fig. S10(c). Very few datapoints were above this value and they occurred towards the end of the experiment, where the particle was completely inverse micellar (Fig. 1(i) in the main text – where there is no lamellar peak and integration of the lamellar peak position range returned the area of the noise around the background, resulting in some large apparent micellar-lamellar peak ratios).
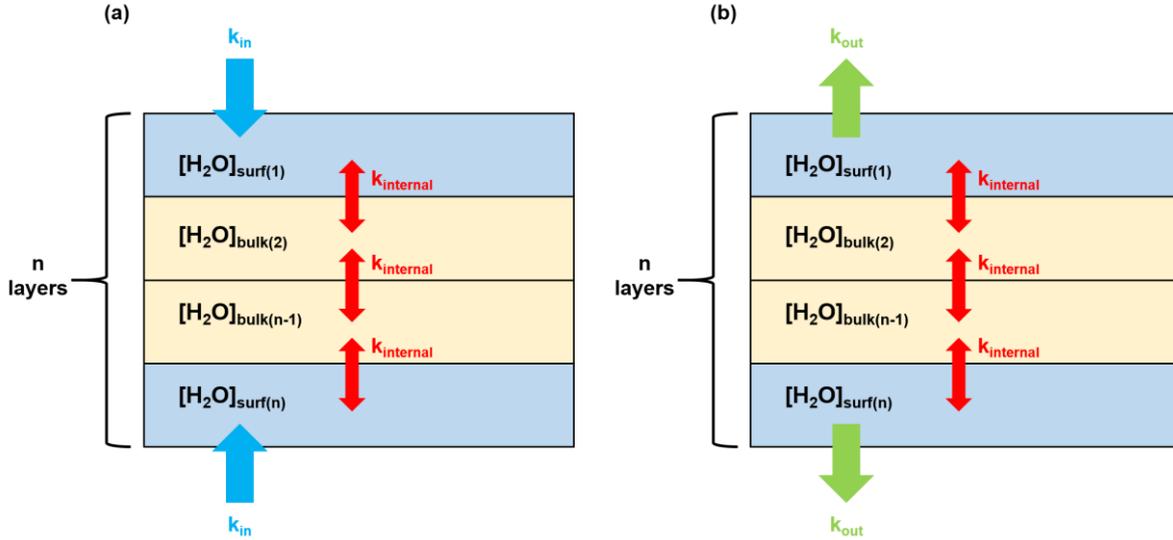
Figure S11. A schematic representation of the water uptake (a) and loss (b) model employed in this study.

Internal water diffusion was evolved in a Vignes-type fashion (*e.g.* Price *et al.*) (Price et al., 2015), relating water diffusion and layer composition (Eq. S1).

$$k_{internal,k} = (k_{micellar})^{\alpha[H_2O]_k}(k_{lamellar})^{1-\alpha[H_2O]_k} \qquad \text{(Eq. S1)}$$

$k_{internal,k}$ is the rate of internal diffusion in layer k; $k_{micellar}$ and $k_{lamellar}$ are the rates of water diffusion in the inverse micellar and crystalline lamellar phases, respectively; α is an activity coefficient which is assumed to be 1, analogous to the assumption of Davies and Wilson.(Davies and Wilson, 2016) $[H_2O]_k$ is the amount of water as a fraction of the maximum water content in layer k, which is assumed to be the equilibrium water content for the inverse micellar phase.

The water uptake model (Fig. S11(a)) is described by Eq. S2 and S3:

$$\frac{d[H_2O]_{surf}}{dt} = k_{in}([H_2O]_{max} - [H_2O]_{surf}) + k_{internal}([H_2O]_k - [H_2O]_{surf}) \qquad \text{(Eq. S2)}$$

$$\frac{d[H_2O]_k}{dt} = k_{internal,k}([H_2O]_{k+1} + [H_2O]_{k-1} - 2[H_2O]_k) \qquad 2 < k < n-1 \qquad \text{(Eq. S3)}$$

The water loss model (Fig. S11(b)) is described by Eq. S4 with internal diffusion described by Eq. S3:

$$\frac{d[H_2O]_{surf}}{dt} = -k_{out}([H_2O]_{surf} - [H_2O]_{min}) + k_{internal}([H_2O]_k - [H_2O]_{surf}) \qquad \text{(Eq. S4)}$$

The model splits the particle into a number of layers equivalent to the number of experimental positions (*n*) measured. The maximum ($[H_2O]_{max}$) and minimum ($[H_2O]_{min}$) amounts of water were set to 1 and 0, respectively in order to fit with the normalised experimental data. Each layer is given a number (*k*) with *k* = 1 & n being the top and bottom surface layers, with their respective amounts of water defined as $[H_2O]_{surf}$ in Eq. S2 & S4. The key parameters varied to fit the model with the data were the rate of water uptake (k_{in} – water uptake), the rate of water loss (k_{out}– water loss), $k_{micellar}$ and $k_{lamellar}$.

This model assumes: (i) constant rate of water uptake/loss into the particle – water uptake is expected to change with changing particle phase, however to avoid adding too many unknown parameters to the model we assume that it does not change; (ii) The particle is relatively flat

and non-spherical – the particles levitated in this study are not spherical and spatially resolved data were of a vertical slice of the particle, the model reproduces this; (iii) there is a negligible rate of water loss during water uptake and *vice versa*; (iv) each model layer is well-mixed with no diffusion/water content gradient. Detailed modelling of differences in water uptake/loss rates into and from particles of different self-assembled phases is beyond the scope of this study and is the subject of ongoing work. The model presented here allows us to estimate the difference in water diffusivity between the inverse micellar and lamellar phases.

A Residual Sum of Squares (RSS) was calculated between the model and experiment and was used as a measure of goodness of fit, with lower values corresponding to better fits. Parameters were varied using a differential evolution algorithm whereby bounds are set for each parameter and parameter values are randomly selected from a population (Wormington et al., 1999). Each parameter is then "mutated" in an iterative process, each time the better-fitting parameter is kept. The algorithm eventually converges to an output which returns the minimum RSS value. The best fitting parameters are summarised in Table S3.

Model	k_{in} / $x10^{-3}$	k_{out} / $x10^{-3}$	$k_{micellar}$ / $x\ 10^{-3}$	$k_{lamellar}$ / $x\ 10^{-3}$	*RSS$_{fit}$*
Uptake	3.9	N/A	590	16	209
Loss	N/A	23	600	18	25

Table S3. Optimised water uptake and loss model parameters with the minimised RSS (RSS_{fit}) quoted for both models.

Although the parameters obtained from the model have no physically meaningful units, the ratio between $k_{micellar}$ and $k_{lamellar}$ is ~ 33, highlighting the large difference in water diffusivity between the inverse micellar and crystalline lamellar phase. We must stress that the model fails to capture the prompt deliquescence well during humidification.

S9. Hexagonal Phase in an Excess-Water Mixture of Oleic Acid/Sodium Oleate
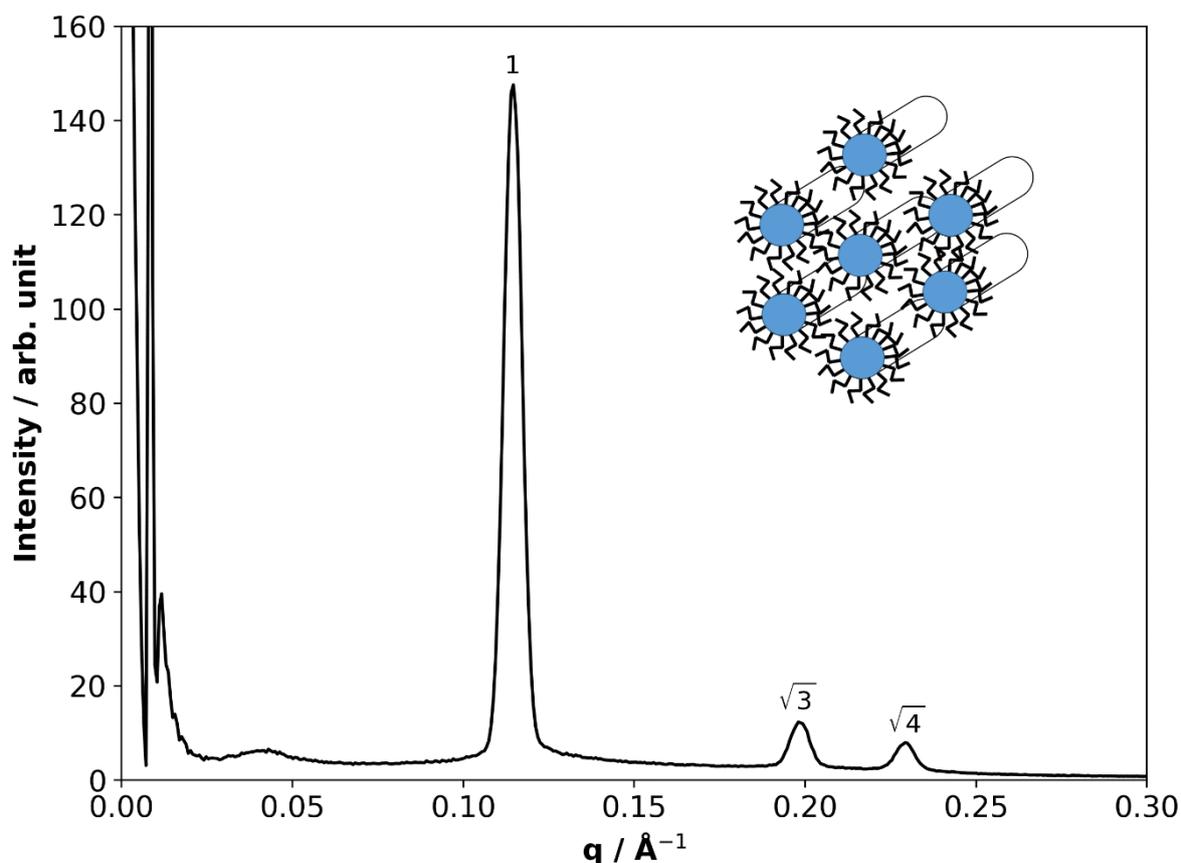
Figure S12. 1–D SAXS pattern of oleic acid-sodium oleate (1:1 wt) mixed with water as a 30 wt % organic mixture. Numbers above the peaks represent the characteristic peak position ratios expected for the inverse hexagonal phase. A cartoon representation of the inverse hexagonal phase is also presented.

It is known that mixtures of this composition make inverse hexagonal arrays of oleic acid-sodium oleate cylinders.(Engblom et al., 1995) This phase can also be envisaged as a hexagonal array of water channels. This is the phase that produces the charcoal texture observed in the POM experiment (Fig. S9(b)). It is likely that this exists if the acid–soap complex is humidified for a time longer than the scope of a synchrotron experiment.

S10. WAXS Pattern of Levitated Oleic Acid
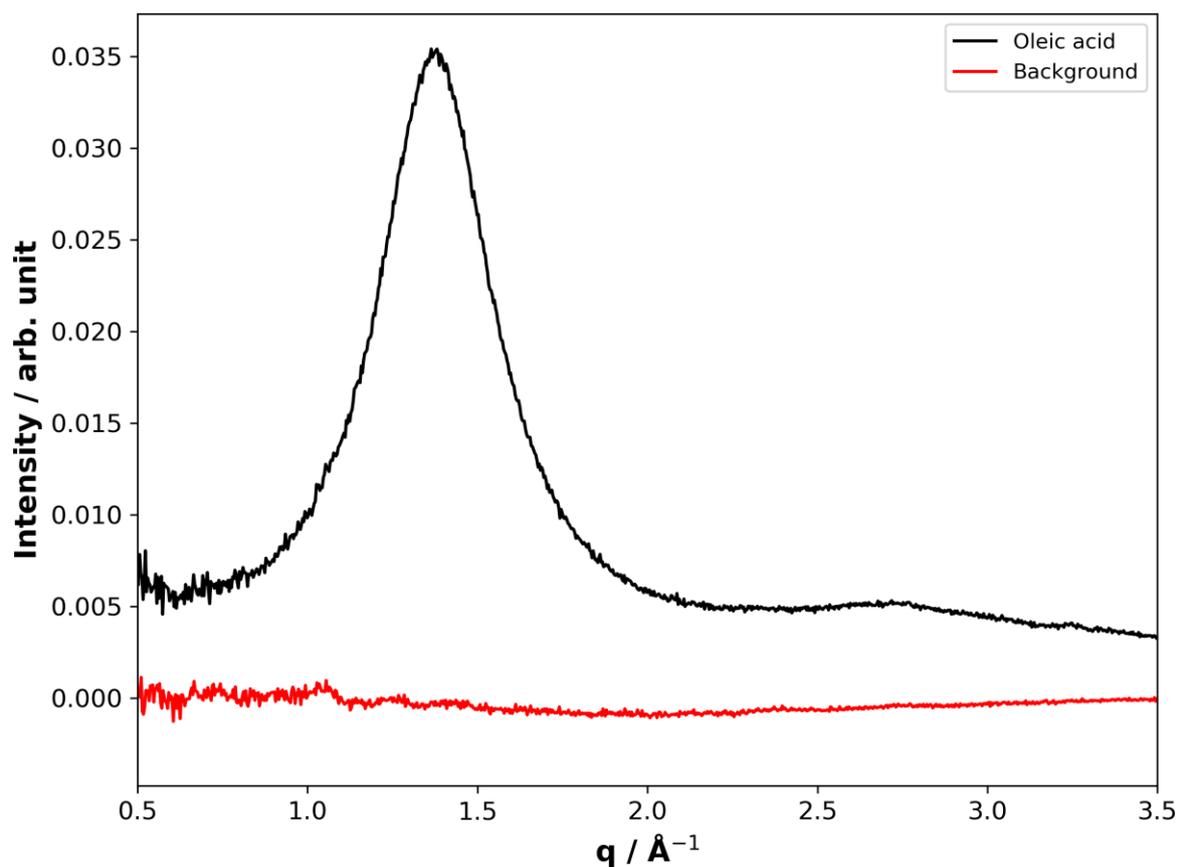
Figure S13. WAXS pattern of the centre of a levitated droplet of oleic acid compared with a background pattern of an empty levitator. This clearly demonstrates that oleic acid has a WAXS pattern. The alkyl chain spacing measured from this pattern is ~ 4.57 Å.

S11. SAXS Pattern of a Levitated Particle of 2:1 wt (Oleic acid : Sodium Oleate) Composition
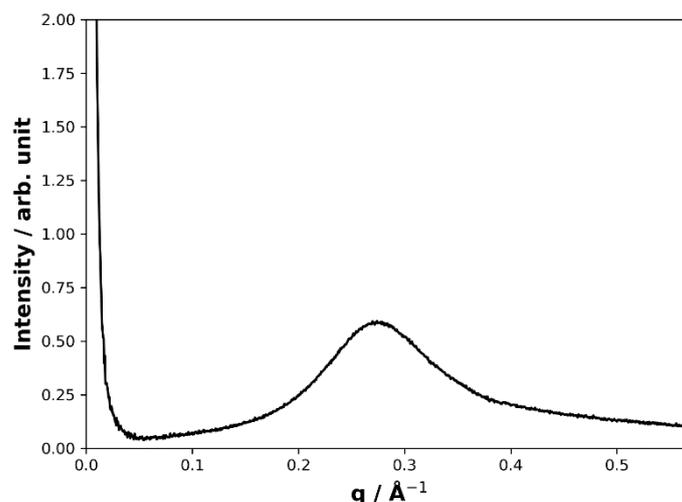
Figure S14. A levitated particle of 2:1 wt (oleic acid : sodium oleate) composition demonstrating a broad peak characteristic of the inverse micellar phase with a *d*-spacing of 36 Å. RH ~ 50 %.

References

Cistola, D. P., Atkinson, D., Hamilton, J. A. and Small, D. M.: Phase Behavior and Bilayer Properties of Fatty Acids: Hydrated 1:1 Acid-Soaps, Biochemistry, 25(10), 2804–2812, doi:10.1021/bi00358a011, 1986.

Davies, J. F. and Wilson, K. R.: Raman Spectroscopy of Isotopic Water Diffusion in Ultraviscous, Glassy, and Gel States in Aerosol by Use of Optical Tweezers, Anal. Chem., 88(4), 2361–2366, doi:10.1021/acs.analchem.5b04315, 2016.

Engblom, J., Engström, S. and Fontell, K.: The effect of the skin penetration enhancer Azone® on fatty acid-sodium soap-water mixtures, J. Control. Release, 33(2), 299–305, doi:10.1016/0168-3659(94)00105-4, 1995.

Lynch, M. L., Pan, Y. and Laughlin, R. G.: Spectroscopic and thermal characterization of 1:2 sodium soap/fatty acid acid-soap crystals, J. Phys. Chem., 100(1), 357–361, doi:10.1021/jp952124h, 1996.

Mantsch, H. H., Weng, S. F., Yang, P. W. and Eysel, H. H.: Structure and thermotropic phase behavior of sodium and potassium carboxylate ionomers, J. Mol. Struct., 324(1–2), 133–141, doi:10.1016/0022-2860(93)08234-U, 1994.

Mele, S., Söderman, O., Ljusberg-Wahrén, H., Thuresson, K., Monduzzi, M. and Nylander, T.: Phase behavior in the biologically important oleic acid/sodium oleate/water system, Chem. Phys. Lipids, 211(September 2017), 30–36, doi:10.1016/j.chemphyslip.2017.11.017, 2018.

Meznarich, N. A. K., Juggernauth, K. A., Batzli, K. M. and Love, B. J.: Structural changes in PEO-PPO-PEO gels induced by methylparaben and dexamethasone observed using time-resolved SAXS, Macromolecules, 44(19), 7792–7798, doi:10.1021/ma2015358, 2011.

Nájera, J. J.: Phase transition behaviour of sodium oleate aerosol particles, Atmos. Environ., 41(5), 1041–1052, doi:10.1016/j.atmosenv.2006.09.016, 2007.

Pfrang, C., Rastogi, K., Cabrera-Martinez, E. R., Seddon, A. M., Dicko, C., Labrador, A., Plivelic, T. S., Cowieson, N. and Squires, A. M.: Complex three-dimensional self-assembly in proxies for atmospheric aerosols, Nat. Commun., 8(1), 1724, doi:10.1038/s41467-017-01918-1, 2017.

Price, H. C., Mattsson, J., Zhang, Y., Bertram, A. K., Davies, J. F., Grayson, J. W., Martin, S. T., O'Sullivan, D., Reid, J. P., Rickards, A. M. J. and Murray, B. J.: Water diffusion in atmospherically relevant α-pinene secondary organic material, Chem. Sci., 6(8), 4876–4883, doi:10.1039/c5sc00685f, 2015.

Seddon, J. M., Bartle, E. A. and Mingins, J.: Inverse cubic liquid-crystalline phases of phospholipids and related lyotropic systems, J. Phys. Condens. Matter, 2, SA285–SA290, doi:10.1088/0953-8984/2/S/043, 1990.

Tandon, P., Förster, G., Neubert, R. and Wartewig, S.: Phase transitions in oleic acid as studied by X-ray diffraction and FT- Raman spectroscopy, J. Mol. Struct., 524(1–3), 201–215, doi:10.1016/S0022-2860(00)00378-1, 2000a.

Tandon, P., Neubert, R. and Wartewig, S.: Thermotropic phase behaviour of sodium oleate as studied by FT-Raman spectroscopy and X-ray diffraction, J. Mol. Struct., 526(1–3), 49–57, doi:10.1016/S0022-2860(00)00441-5, 2000b.

Tandon, P., Raudenkolb, S., Neubert, R. H. H., Rettig, W. and Wartewig, S.: X-ray diffraction and spectroscopic studies of oleic acid-sodium oleate, Chem. Phys. Lipids, 109(1), 37–45, doi:10.1016/S0009-3084(00)00207-3, 2001.

Wormington, M., Panaccione, C., Matney, K. M. and Bowen, D. K.: Characterization of structures from X-ray scattering data using genetic algorithms, Philos. Trans. R. Soc. London A A, 357, 2827–2848, 1999.